Materialia 4 (2018) 575–584

Contents lists available at ScienceDirect

Materialia

journal homepage: www.elsevier.com/locate/mtla

Full Length Article

Long-time point defect diffusion in ordered nickel-based binary alloys: How small kinetic differences can lead to completely long-time structural evolution

Sami Mahmoud*, Normand Mousseau*

Département de physique and Regroupement québécois sur les matériaux de pointe, Université de Montréal, C.P. 6128, Succursale Centre-Ville, Montréal, Québec H3C 3J7, Canada

ARTICLE INFO

Keywords:
K-ART
Nickel alloys
Vacancy
Interstitial
Long-time diffusion

ABSTRACT

In this paper, we characterize the effect of defect kinetics on the stability of ordered nickel-based binary alloys, NiFe, NiCo and NiCu, using the kinetic Activation-Relaxation Technique (k-ART), an unbiased off-lattice kinetic Monte Carlo method with on-the-fly catalog building, that can provide kinetic pathways over second scales taking full account of chemical and elastic effects. We generate the full energy landscape surrounding vacancy and self-interstitial diffusion for $L1_0$ NiFe, an alloy with promising magnetic properties, with those of model $L1_0$ NiCo and NiCu, and combine this information with unbiased long-time kinetic simulations to characterize the link between specific microscopic diffusion mechanisms and overall phase stability. Our simulations demonstrate an unexpected richness and diversity: even though these alloys display similar proprieties like atomic radius, single vacancy and interstitial diffuse along totally different pathways that explain the relative stability of ordered structure.

1. Introduction

With their low expansion at high temperatures and their high resistance to corrosion, nickel based alloys play an important role in high-tech industries such as aerospace and nuclear energy. As demand for more sophisticated materials grows and new manufacturing methods are developed, some of these alloys are also attracting more and more attention for new applications across a wider range of industrial sectors. This is the case, in particular, for chemically-ordered alloys, such as FeNi, that can be grown by Alternate Monoatomic Layer deposition [1] or Molecular Beam Epitaxy (MBE) [2] making them good candidates for applications such as spintronics [3] and inexpensive permanent magnets [4].

These possible applications have caused a renewed fundamental interest to characterize the NiFe and related binary alloys both experimentally [5–7] and numerically [8,9], providing new insights regarding the link between defect kinetics and stability in these systems. While the reported order-disorder transition transition temperature in tetrataenite ($L1_0$ NiFe) is 593 K, Bordeaux et al. showed that the slow disordering, characterized by a 3.1 eV activation energy, pushes the kinetic transition to much higher temperatures. Yet, Geng et al. showed that room temperature mechanical milling can overcome these barriers and lead to the production of nanocrystalline $L1_0$ NiFe from the disordered phase. Comparing vacancy diffusion between ordered and disordered NiFe, TiAl and CuAu, in high temperature molecular dynamics, find that, for ordered systems, the antisite creation rate is highly composition dependent.

These works underline the importance of understanding the slow kinetics associated with the general class of $L1_0$ alloys and, more particularly, NiFe alloys, by capturing the detailed kinetics of vacancy and mass diffusion in these materials. Yet, the slow defect diffusion has made it difficult to characterize the nature of point defect diffusion in these alloys by standard techniques, such as molecular dynamics, and how it differs from that, much better understood, observed in perfect systems. [10] To overcome this limitation, we revisit this problem using the kinetic Activation Relaxation Technique (k-ART) [11,12], an off-lattice kinetic Monte Carlo methods with unbiased on-the-fly event catalog construction capabilities, to describe in details the kinetic of point defects and their associated energy landscape in Ni-based alloys comparing, in particular, with their behavior in pure iron [13] and nickel [10] gained recently, with the same technique.

More precisely, in order to understand the link between point defect kinetics and structural evolution and kinetic stability, we consider three ordered $L1_0$ model systems NiFe, NiCu and NiCo, where only $L1_0$ NiFe is found experimentally to be thermodynamically stable. The full energy landscape associated with single point-defect diffusion is reconstructed

* Corresponding author.
E-mail addresses: sami.mahmoud@umontreal.ca, samimahmoud@live.com (S. Mahmoud), normand.mousseau@umontreal.ca (N. Mousseau).

https://doi.org/10.1016/j.mtla.2018.11.013
Received 13 November 2018; Accepted 18 November 2018
Available online 22 November 2018

for each system and long-time k-ART simulations are launched ot generate kinetic trajectories at 300 K, far away from the NiFe order-disorder transition, to better establish the inherent differences and similarities between the alloys. We also characterize the landscape and kinetics of these alloys under interstitial diffusion as even though the evolution of these alloys seems mostly controlled by vacancies, the preparation of $L1_0$ NiFe phase through ion bombardment [14] or mechanical milling [7] will generate interstitials that will play a role in the phase ordering.

In this work, long-time k-ART simulations are performed using empirical potential to fully characterize the diffusion kinetics and energy landscape of single vacancies and interstitials in $L1_0$ NiFe, NiCo and NiCu alloys. As potentials need to be validated for the type of problem studied, we first compare three sets of parameters for NiFe based on the Embedded Atom Method formalism (EAM) [15] developed by Bonny and collaborators to identify the most appropriate set of parameters. Simulations show that the energy landscape surrounding the defects and the associated kinetics vary greatly as a function of alloy composition, leading to leading to very different consequences on the structural evolution of these alloys and opening the door to design more stable and even self-annealing materials through kinetic control.

2. Methods

2.1. Kinetic-Activation Relaxation Technique (k-ART)

The kinetic Activation Relaxation Technique (k-ART) [10–12] is an off-lattice kinetic Monte Carlo method based on the Activation-Relaxation Technique (ART nouveau) [16,17] for event searching and NAUTY [18] for topological analysis and generic classification. The flowchart in Fig. 1 shortly explain the k-ART method. While details about k-ART can be found elsewhere [11,19,20], its basic principles can be summarized briefly as follow.

After classical local energy minimization of the total structure using FIRE (Fast Inertial Relaxation Engine) [21], k-ART characterizes the local topological environment surrounding each atom with the help of NAUTY. For this, all atoms contained within a sphere of a given radius (6 Å for the current system) are extracted. A graph is generated by drawing edges between all atoms within a cut-off distance of 2.8 Å of each other, corresponding roughly to including first-neighbors only. Additional self loops are added to distinguish between the various atomic species. The graph, containing about 80 vertices, is then sent through NAUTY to extract an identifier associated with its automorphic class. If the topology is known and cataloged, generic events associated with it are placed in event tree, otherwise 50 ART nouveau searches are launched to identify its associated events; additional searches are added in some cases to ensure the completeness of the catalog. To ensure that the events correspond to connected sets of minimum-saddle-minimum states, a relaxation is performed in both direction form the saddle point. After identifying all events, a first evaluation of the time to the next event is performed according to transition state theory [22] with a constant 10 THz prefactor. All barriers in the tree with an occurrence probability of one in 10,000 or higher are reconstructed and fully relaxed to ensure that all elastic events are exactly included. After this relaxation, the time step is evaluated again and the clock moved forward following the Poisson distribution characterized by this time step. An event is then selected at random with a probability proportional to its rate and the system is ready for the next step. To prevent being trapped by events with low-energy non-diffusive barriers known as flickering states, we use the basin-accelerated mean-rate method (bacMRM) [23], which solves analytically intra-basin kinetics. Since the right kinetics is maintained, it is possible to adjust the threshold for defining flickering states depending on alloy nature and defect type without affecting the result. In the case of vacancies, with high migration energy for all systems, this threshold is set at 0.5 eV. For interstitials, with migration energy and oscillations activation energies are small (around 0.05 eV), the bacMRM threshold is set to 0.01 eV.

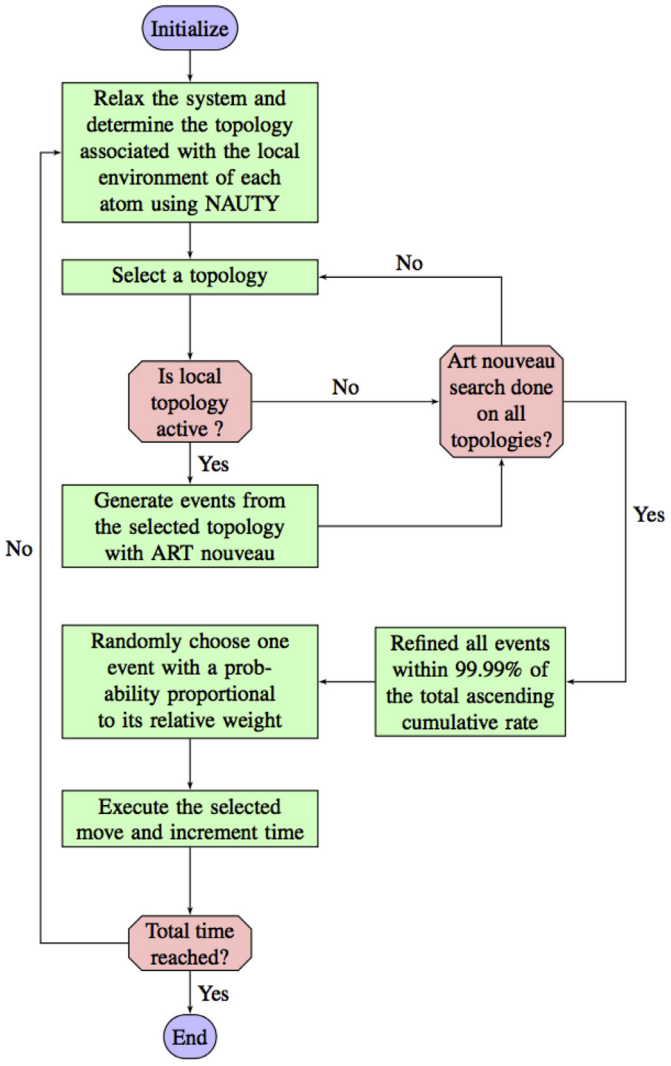

Fig. 1. Flowchart of k-ART.

Table 1
Lattice parameters of pure metals considered for comparison and alloys (NiFe, NiCu and NiCo) used in this study. *d* is the interatomic distance.

Metal	*a*	*b*	*c*	*d*	Crystal structure	reference
pure Ni	3.5200	3.5200	3.5200	2.48	fcc	[10]
pure Fe	2.8665	2.8665	2.8665	2.87	bcc	[26]
pure Cu	3.6147	3.6147	3.6147	2.56	fcc	[27]
pure Co	2.5071	2.5071	4.0695	2.51	hcp	[28]
NiFe	3.5790	3.5790	3.5790	2.53	$L1_0$ fcc	[8]
NiCu	3.5594	3.5594	3.6483	2.52	$L1_0$ tetragonal	[25]
NiCo	3.5250	3.5250	3.5250	2.49	$L1_0$ fcc	[8]

2.2. Simulated systems

We consider three Ni*X* alloys — NiFe, NiCo and NiCu — all at a 50–50% concentration in both fcc and $L1_0$ structure. The simulated systems are cubic boxes of 4000 atoms, a size sufficient to ensure that defect diffusion is not affected by boundary effects, relaxed at zero pressure; lattice parameters for these three cells are indicated in Table 1. Simulations are performed at 300 K, as indicated below, far from the order-disorder transition temperature for NiFe established experimentally at 600 K. Vacancies of Ni or/and *X* are created by removing one atom of the given species. Interstitial atoms, for their part, are placed initially in

Table 2
Migration energy of one vacancy in NiFe alloy as a function of first nearest-neighbor (1 nn) environment composed by (*n, m*) elements where *n* and *m* are the number of Ni and Fe, respectively. Considered cases here are (8,4) ↦ (8,4) for the diffusion of Fe vacancy in Fe plane, (4,8) ↦ (4,8) for the diffusion of Ni in Ni plane and (8,4) ↦ (5,7) for the jump of Fe vacancy from the Fe to the Ni plane. All vacancy diffusion mechanisms consist of direct 1 nn jump except for values with an asterisk (*) that correspond to a two-step diffusion to 1 nn position. All values are in eV.

	Bonny 2009	Bonny 2011	Bonny 2013	DFT
(8,4)↦(8,4)	0.75	1.00	0.77*	0.87 [9]
(4,8)↦(4,8)	1.07	1.32	0.55*	1.05 [9]
(8,4)↦(5,7)	1.12	1.22	1.09	1.07 [8], 1.31 [9]

an octahedral site and, after minimization, form a dumbbell with one of their neighbors, either the same type or not.

For the $L1_0$ structure, Ni and *X* atomic layers are stacked alternatively along the ⟨100⟩ direction. It has been shown experimentally [2,4] and from DFT calculation [24] that the NiFe-alloy $L1_0$ structure is stable. While this is not the case for the two other alloys, [1,25] comparing diffusion pathways of point defects in these three cases contributes to providing an explanation for the observed difference in stability in addition to serving as a reference system for understanding diffusion in solid solutions.

2.3. Choice of parameters for the interaction potential

To select the best available forcefield for our simulation, we first compare various parameter sets optimized by Bonny and collaborators within the embedded-atom method framework for NiFe [29–31], NiCo [32] and NiCu [33] systems.

Because NiFe alloy has received more attention than the two other systems, we focus on this alloy to establish the best potential, comparing three sets of parameters with available DFT results. Table 2 shows results obtained with three potentials for vacancy diffusion barriers in three different first nearest-neighbors (1 nn) environments as well as recent DFT calculations [8,9]. Bonny's 2013 EAM potential introduces an unphysical two-step mechanism for monovacancy diffusion where the vacancy, starting from the crystalline position, finds a first minimum halfway on the path to the 1 nn site localized in the same plane nature. This mechanism is observed for both Fe and Ni vacancies with barriers of 0.87 and 1.05 eV, respectively as indicated in Table 2. Bonny's 2009 EAM potential under-estimates the intraplanar in Fe layer and the interplanar diffusion barriers by 0.12 and 0.19 eV, respectively, compared to Chakraborty's [9] DFT results. Since DFT calculations between various groups disagree for the interplanar diffusion (8,4) ↦ (5,7), we take as reference the average between the two values; here again, Bonny's 2011 potential presents the best value. Finally, Zhao et al. [8] have compared the distribution of formation energies in random alloys as a function of first-neighbor environment for DFT and empirical potential and concluded that, although imperfect, Bonny's 2011 offer the best agreement with *ab initio* results. Overall, therefore, Bonny's 2011 EAM potential offers reasonable accuracy and better relative energies that the other empirical potentials and is selected here for the treatment of NiFe alloy.

2.4. Formation energy

The formation energy $E^{conf}_{f1SIA}(NiX)$ for a mono-self-interstitial (1SIA) in NiX (X is Fe or Cu or Co) alloy is calculated as follow:

$$E^{conf}_{f1SIA}(NiX) = \left(E^{conf} - \left(E_p \times \frac{(n+1)}{n}\right)\right),$$

where E^{conf} is total energy of the system in the considered configuration, E_p is the energy of the perfect crystal with *n* atoms (4000 in our case). According to this definition, a state with lower $E^{conf}_{f1SIA}(NiX)$ is more stable.

3. Results

3.1. Vacancy diffusion

To characterize monovacancy diffusion in $L1_0$ structure, we need information on the eight barriers presented in Fig. 2. Four barriers are associated with intraplanar migration depending on the plane and vacancy types, and four others determine the interplanar ones that depend on vacancy type and the initial and final hosting plane. Table 3 presents all k-ART generated barriers for the three alloys.

We first focus on the NiFe case. For this alloy, the lowest barrier, at 0.81 eV, corresponds to a nickel vacancy jump from the Ni to the Fe plane. Once in this plane, the Ni vacancy diffuses preferably in Fe plane with a barrier of 1.03 eV. Indeed, although the jump to the Ni plane is only slightly higher, a 1.13 eV, Ni vacancy intraplanar diffusion in the Ni plane involves crossing a much higher energy barrier, at 1.32 eV, 0.25 eV greater than for pure Ni [10]. A Ni vacancy, therefore, would create a single Fe antisite in the Ni, before diffusing in the Fe sublayer. To avoid obscuring the results, we will label the various sites caused by an initial vacancy by the initial defect (here Ni vacancy), understanding, for example, that it means an Fe antisite with Fe vacancy when it is in the configuration just described.

We observe a similar behavior for the Fe vacancy, which diffuse preferably in the Fe layer, crossing a barrier of 1.00 eV. The Fe vacancy will only rarely jump to the Ni layer, as it requires an energy of 1.22 eV, with diffusion in this layer ever higher, at 1.25 eV due to the presence of an antisite in the Fe layer.

The integrated effect of this landscape surrounding a monovacancy in the $L1_0$ NiFe alloy, obtained by long-time k-ART simulations, is presented in Fig. 3(a). The graph shows an evolution dominated by intraplanar diffusion in the Fe layer (Y and Z directions), with almost no interplanar motion as that the vacancy diffuses in an environment dominated by Ni atoms (4 Fe in plane and 8 Ni out of plane). This conclusion is confirmed by the right-handed panel (Fig. 3(d)). This figure presents the events generated along the pathway as dots positioned as a function of the initial energy (measured with respect to the ground state, *x*-axis), the final energy (*y*-axis) and the energy barrier (colored according to the right-handed color code). We see, for example, that for symmetric events, at (0,0), the connecting barrier is light yellow or 1.32 eV; similarly, an event starting in a state at 0.3 eV above GS, can reach the ground state (0.3, 0) after crossing a 1.22 eV barrier. This plots shows all 2500 accepted events generated during the 4.5 million second (1250 h) run at 300 K, with a typical rate of 2.2×10^{-7} s^{-1}. The small number of differently positioned points on the graph indicates that only a few different states are visited, and that the system does no show structural evolution, remaining essentially ordered as the vacancy diffuses around, restricted essentially to the Fe planes. As temperature increases, however, as observed experimentally, the relative probability between the jumps in different orientations is reduced and leads to disordering. As temperature is raised to 600 K, for example, near the experimental order-disorder temperature, interlayer jumps takes place every 100 to 300 μs (not shown), while no interlayer jump was observed in a 10^6 s run at 300 K.

Vacancy diffusion in the $L1_0$ NiCo alloy is opposite to that of the NiFe case. From Table 3, the fastest move for the Ni vacancy is towards the Co sublayer, with a 0.77 eV barrier, compared with 1.07 eV for Ni intralayer diffusion. Once in the Co layer, the vacancy is more likely to diffuse in plane (1.04 eV barrier) than to come back to the Ni layer (1.20 eV). However, the Co vacancy will preferably move to the Ni plane, with a 0.75 barrier, rather than diffuse intraplane (with a barrier of 1.19 eV). Once in the Ni plane, however, it can move easily within the plane, with a 0.83 eV barrier. For NiCo, therefore, a vacancy will first move to the other plane, creating an antisite, then diffuse intraplane until it moves away from this antisite and prefers, then, to cross into a new plane, leading to the multiplication of antisites and the disordering of planar structure.

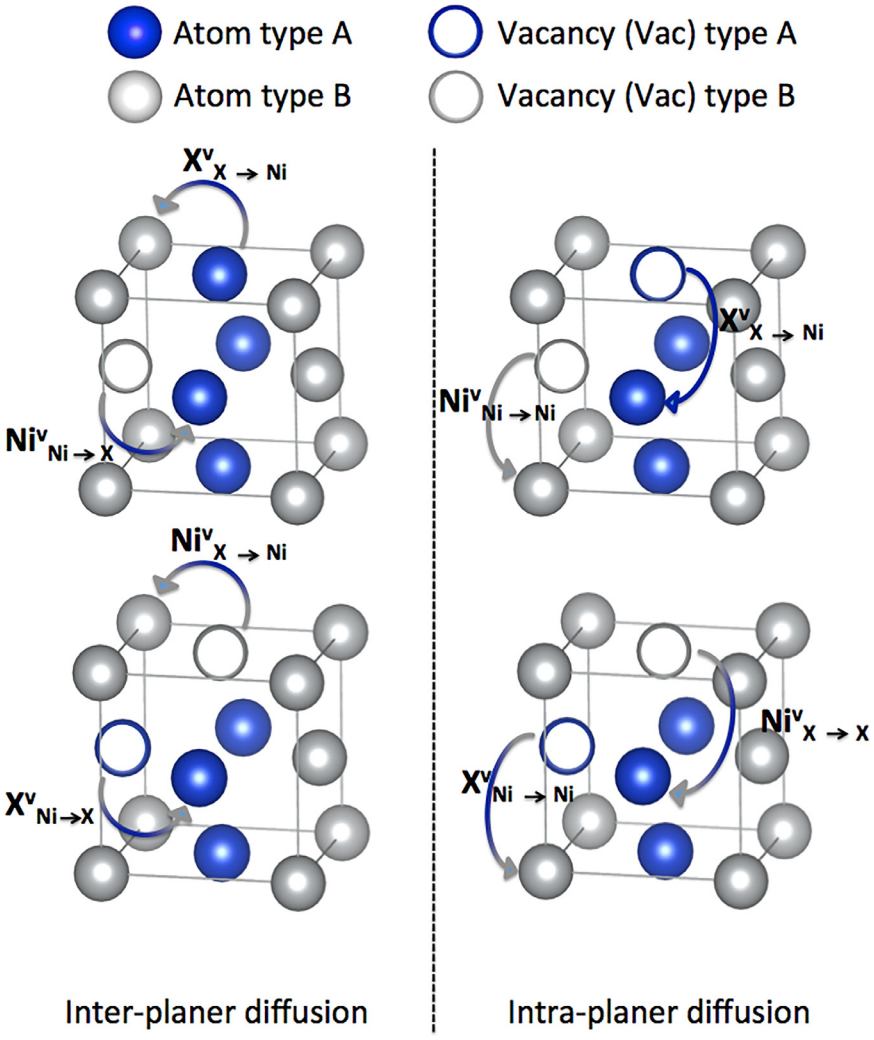

Fig. 2. Interplanar and intraplanar diffusion pathways of a vacancy diffusing in fcc $L1_0$ alloys. While intraplanar jumps are symmetric, this is not the case for interplanar diffusion that generates antisites, as indicated on the left-hand-side panel.

Table 3
Migration energies of single vacancy in L_{10} fcc nickel binary-based alloys. Notation is a bit similar to Kröger–Vink's ones (Exemple : $Ni^v_{X \to Ni}$ is the barrier for the Ni vacancy (v) to diffuse from the X plane (Fe or Co or Cu) to the Ni plane).

Alloy/Barrier	$Ni^v_{Ni \to X}$	$Ni^v_{X \to Ni}$	$Ni^v_{Ni \to Ni}$	$Ni^m_{X \to X}$	$X^v_{X \to Ni}$	$X^v_{Ni \to X}$	$X^v_{X \to X}$	$X^v_{Ni \to Ni}$
NiFe	0.81	1.13	1.32	1.03	1.22	1.22	1.00	1.25
NiCu	0.65	0.53	0.89	0.56	0.65	0.84	0.57	0.94
NiCo	0.77	1.20	1.07	1.04	0.75	1.22	1.19	0.83

This analysis is confirmed by looking at the long-time diffusion of a monovacancy in the $L1_0$ NiCo alloy, starting from a perfectly ordered system as presented in the left-handed panel of Fig. 3(c). Diffusion shown here is over 70 s and 1200 steps is almost perfectly isotropic, as indicated by a similar diffusion along the three axes. Looking at the event's characteristics (Fig. 3(f)), we note that, contrary to both NiFe and NiCu, for which the system's total energy does not evolve over the simulation time scale, for NiCo, the total energy drops by more than 10 eV, over 70 s, as the vacancy diffuses around and disorders the alloy, crossing barriers that vary by at most 0.30 eV, as a function of the local environment, in agreement with recent DFT result that show antisites are energetically favored in this alloy [34].

The diffusion behavior of vacancy in NiCu alloy is also different from the two other alloys. For this system, the evolution of this point defect takes place almost isotropically, as indicated in Fig. 3(b), because of similarities in barriers between the various mechanism and thus specific pathway dominates: the lowest barriers correspond to a migration of Ni vacancy from Cu to Ni plane and intraplaner Cu vacancy in Cu plane with barriers of 0.53 and 0.57 eV, respectively. The migration of Ni or Cu vacancy from a layer to another one of different type require crossing 0.65 eV, higher than for the two other mechanisms, but still much lower than for the two other alloys, and lower also than for pure copper with an activation energy equal to 0.74 eV [35]. Fig. 3(e) shows that, contrary to NiCo, disordering does not lower the total energy but takes place for entropic gains. As for NiCo, however, the 1246 events taking place over 80 s in NiCu cross barriers that vary as a function of local chemical environment, leading to the scatter observed in in Fig. 3(b).

3.2. Interstitial diffusion

For the three alloys considered, the interstitial atom shares a crystalline site with a lattice-atom, forming a dumbbell with a formation

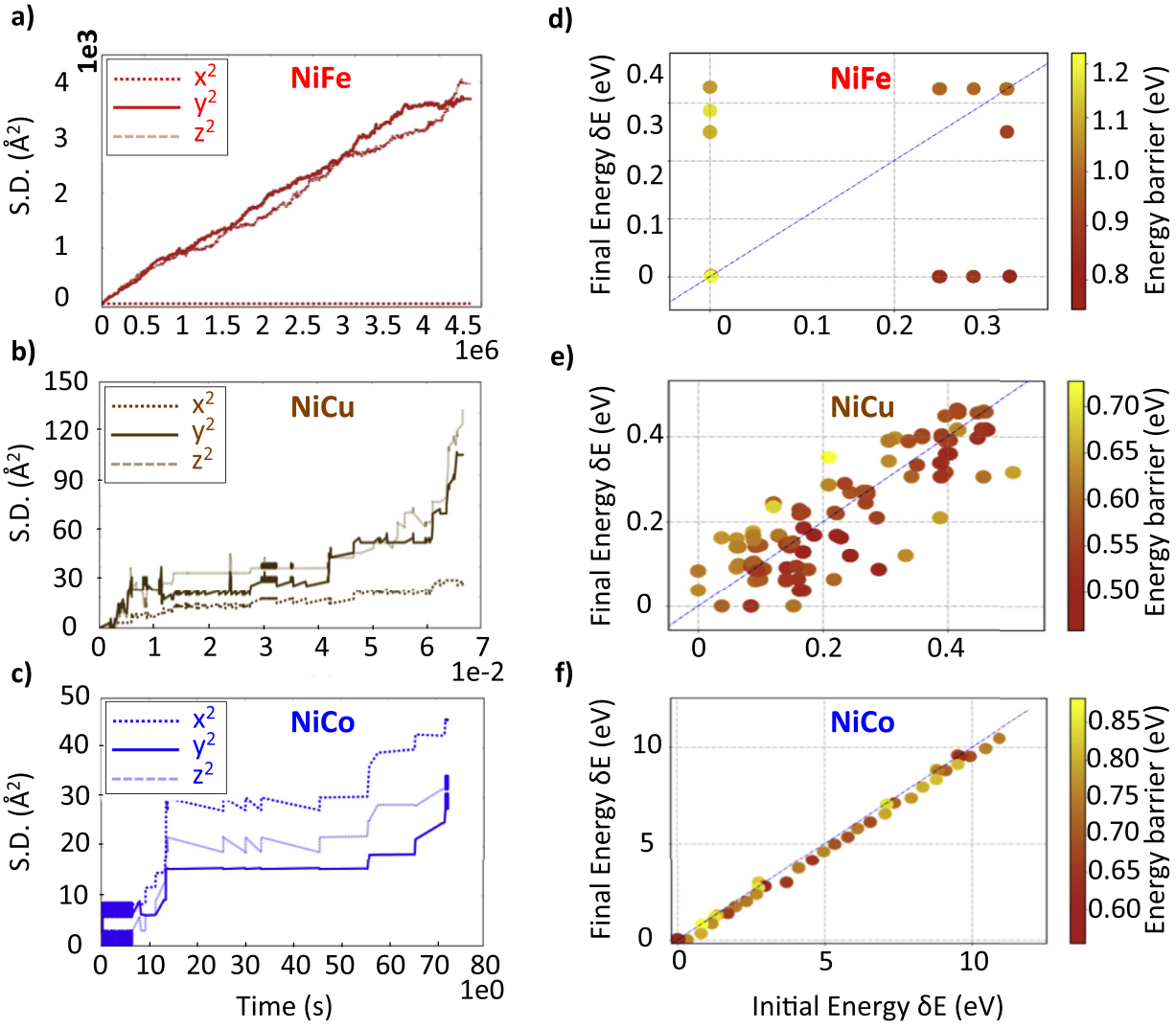

Fig. 3. Diffusion of vacancy in ordered $L1_0$ NiFe, NiCu and NiCo alloys. Left-hand-side panels (a,b,c): Square displacement (S.D.) as a function of time and lattice directions (*y* and *z* represent the elemental planes, with *x*, pointing in the normal direction); right-hand-side panels (d,e,f): final energy of each accepted event as a function of initial energy, as measured from the ground state. The symbol color indicates the energy barriers as defined by the scale on the right-hand side of the graph. (For interpretation of the references to color in this figure, the reader is referred to the web version of this article).

Table 4
Formation energies of mono-interstitial in $L1_0$ alloys as a function of dumbbell composition, orientation and belonging plane. Letters *p* and *h* followed by an atom type means perpendicular and horizontal to the atom type plane, respectively. The presence of an asterisk (*) means that the dumbbell is unstable and that the energy given is for the nearest metastable state the system relaxes into. All values are in eV.

Dumbbell composition	*NiNi* dumbbells				*NiX* dumbbells				*XX* dumbbells			
Belonging plane and orientation	*pNi*	*hNi*	*pX*	*hX*	*pNi*	*hNi*	*pX*	*hX*	*pNi*	*hNi*	*pX*	*hX*
NiFe	3.14	3.38	3.32	3.59	3.82	3.90	3.62	3.63	4.48	4.26	3.72	4.27
NiCu	1.36	1.22	1.39	1.40	2.40	1.98	2.02	2.31	2.92*	2.84	2.86	3.44
NiCo	4.09	3.32	3.00	3.48	5.50	3.34*	4.46*	5.54	5.06	4.89	5.80	6.17

energy that is influenced by the dumbbell composition, orientation and its insertion plane, for a total of 12 theoretical different conformations for each alloy, as shown in Table 4, that provides the formation energy for these various configuration. For NiFe alloy, all twelve dumbbells can be stabilized. This is not the case for the other alloys: the CuCu dumbbell perpendicular to the Ni monolayer in NiCu as well as the NiCo dumbbells, either perpendicular to Co layer or in the Ni layer layer, and rather flip directly into a different orientation or form a different dumbbell.

As seen from this table, dumbbells are easiest to form in NiCu, often by a considerable margin, while they are much less sensitive to environment for NiFe : 1SIA formation energies for NiCu, NiFe and NiCo alloys are in the range of [1.22 eV,3.44 eV], [3.14 eV,4.48 eV] and [3.00 eV,6.17 eV], respectively. For the three alloys, the NiNi dumbbell is always more stable than dumbbells composed of Ni and the alloying element in agreement with recent *ab initio* calculations [36]. They show relatively narrow energy range as a function of their position (Ni or X

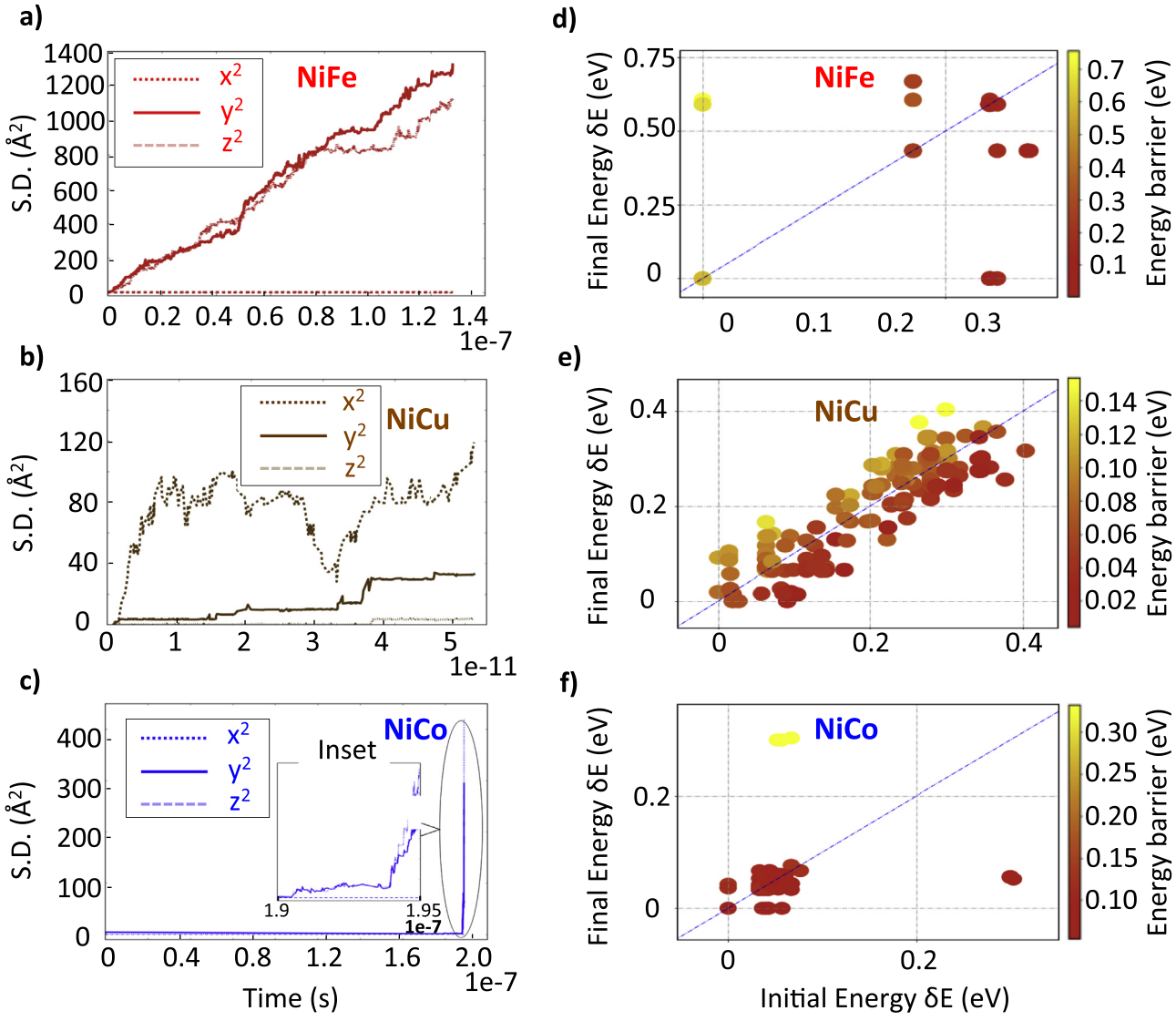

Fig. 4. Diffusion of interstitial in ordered $L1_0$ NiFe, NiCu and NiCo alloys. Left-hand side panels (a,b,c): square displacement (S.D.) in Å as function of time and directions; right-hand-side panels (d,e,f): final energy as a function of initial energy, measured from the ground state. The symbol color indicates the energy barriers as defined by the scale on the right-hand side of the graph.

plane) and orientation, except for NiNi with a parallel orientation in the Ni plane for NiCo, that is 0.77 eV above the NiNi dumbbell with a parallel orientation in the Co plane.

After characterizing the thermodynamical properties of 1SIA in the three alloys, we turn to their kinetics and its effects on their structure. As shown in Fig. 4, the direction of 1SIA dumbbells migrations is alloy dependent, leading to many more possible pathways, as suggested in Table 5, which displays the activation barriers for SIA diffusion in NiFe. Because of the complexity of the energy landscape associated with the structure, however, many pathways — transition or final states — that would be present in pure Ni FCC are not found here: starting from the expected final state, the system relaxes in only a restricted number of configuration. For NiFe, (Fig. 5), the dominant diffusion movement is a translation-rotation (also named shift-rotation [8]) mechanism in the Ni plane with an energy barrier of 0.23 eV, starting from a dumbbell parallel to the Ni plane. The perpendicularly oriented dumbbell, corresponding to the ground state, requires an additional 0.52 eV to turn. Making a translation-rotation to reach the NiNi$\langle 010\rangle_{Ni}$ (or NiNi$\langle 001\rangle_{Ni}$) is easier than the direct translation from Ni plane to its nearest Ni plane that cost 0.62 eV as energy barrier (not shown in the table). Starting from NiNi$\langle 010\rangle_{Ni}$, the complex can diffuse easily by successive translation-rotation to reach NiNi$\langle 001\rangle_{Ni}$ (or vice versa) in Ni layer after crossing 0.23 eV. The NiNi$\langle 010\rangle_{Ni}$ dumbbell (or NiNi$\langle 001\rangle_{Ni}$) can also translate-rotate to form NiFe$\langle 010\rangle_{Fe}$ after crossing 0.27 eV. At 300 K, as

Table 5
Activation barriers of SIA diffusion by translation-rotation mechanism in NiFe alloy depending on dumbbell composition and plane belonging. Barriers connecting in an unstable state are not indicated. Symmetrically-possible transition that do not exist due to instability of the initial or/and the final state, or because of the need for a non-available antisite in one of states are indicated as n/e. All values are in eV.

To\From		Ni plane			Fe plane		
		NiNi	NiFe	FeFe	NiNi	NiFe	FeFe
Ni plane	NiNi	0.23	n/e	n/e	0.27	0.03	–
	NiFe	n/e	n/e	0.16	n/e	0.16	0.44
	FeFe	n/e	0.15	n/e	n/e	n/e	0.24
	NiNi	0.31	n/e	n/e	n/e	n/e	n/e
Fe plane	NiFe	0.27	0.15	n/e	n/e	n/e	n/e
	FeFe	n/e	0.50	0.38	n/e	n/e	n/e

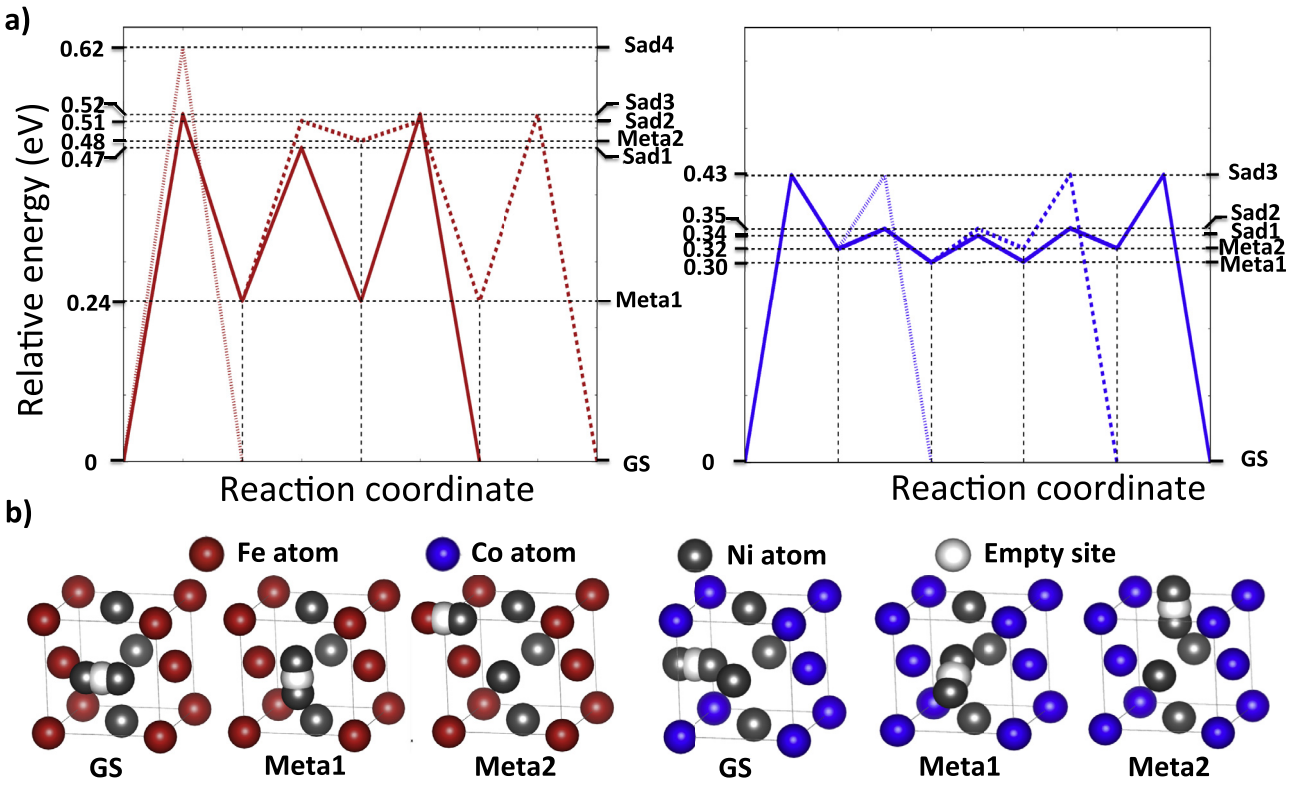

Fig. 5. Shortest self-interstitial diffusion pathways in ordered NiFe (red) and NiCo (blue) alloys. (a) The first (continuous line), the second (dotted line) and the third (dashed line) dominant mechanisms. (b) Atomic arrangement in the ground (GS), metastable (Meta1 and Meta2) and saddle (Sad1 and Sad2 and Sad3 and Sad4) states. Dumbbells can be seen as two atoms connected by an empty site. (For interpretation of the references to color in this figure legend, the reader is referred to the web version of this article).

shown in Fig. 4(a), over a 10^{-7} s, the interstitial, diffuses essentially in the Ni layer, a preference that decreased significantly with temperature: from 300 to 600 K, near the order-disorder temperature, the ratio between diffusion rates in the type layers falls from about 1 to 1000 to 1 to 30. At 300 K, the system diffuses mostly between states above GS — only 1% of the events are directly connected to the GS (where the systems spends 56% of the simulation time). Most of the diffusion — about 70% of the jumps — takes place along the the meta1-meta1 pathway defined in Fig. 5, with a 3.1 Å averaged displacement between minima. About 15% of the transitions take place through the meta1-meta2 pathway, with jumps of 3.0 Å. From meta2, the transition symmetry prevents the NiFe$\langle 001\rangle_{Fe}$ dumbbell to move directly to the ground state, it must therefore go back to the meta1 state a step performed 14% of the time.

For NiCu, interstitial diffusion is also dominated by translation-rotation mechanisms with migration barriers much lower than for NiFe : between 0.03 and 0.16 eV, as indicated in Table 6. 1SIA diffusion is therefore much faster than the case of NiFe alloy, taking place on picosecond timescale at 300 K, similar to interstitial diffusion in pure Cu (0.11 eV) [37]. Contrary for NiFe, however, all diffusion directions are almost equivalent and barriers do not depend strongly on the dumbbell composition; this is reflected, in part, in the different subset of accessible pathways for the 1SIA than observed in NiFe. The first observed mechanism that does not correspond to a translation-rotation is a direct translation in $\langle 100\rangle$ (or equivalent), with 0.39 eV barrier, significantly higher than the dominant ones. As shown in Fig. 4(b), diffusion in z direction is less probable than in plane due to a slightly larger distance between atoms for this direction than in the others. With these barriers, 1SIA diffusion in NiCu is therefore almost isotropic contributing to the disordering of the crystal.

For NiCo, NiNi crowdion motion dominates the diffusion as indicated in Fig. 5. Starting from the GS characterized by $\langle 100\rangle_{Co}$ NiNi dumbbell, the defect go to a $\langle 001\rangle_{Ni}$ NiNi dumbbell conformation (0.32 eV above GS and characterized by a perpendicular dumbbell in Co layer) through a translation-rotation after crossing a 0.43 eV barrier (Table 7). Once in $\langle 001\rangle_{Ni}$, the dumbbell of NiNi adopts a crowdion configuration along the $\langle 011\rangle_{Ni}$ direction (0.30 eV above GS), after crossing a small 0.03 eV barrier and can then diffuse rapidly in the same direction (Ni plane) crossing small 0.04 eV barriers or moving between $\langle 011\rangle_{Ni}$-crowdion and $\langle 001\rangle_{Ni}$ dumbbell states with a limiting barrier of 0.05 eV which corresponds to a timestep of few picoseconds per jump. While these states are well above GS, moving NiNi$\langle 001\rangle_{Ni}$ dumbbell back to $\langle 100\rangle_{Ni}$ is harder than the 0.11 eV would let expect as this jump can only take place in the presence of a Ni antisite in the Co layer, as the NiCo not only because it requires a higher barrier (0.11 eV), but also it requires the existence of a neighbor Ni atom in Co layer to form. Without it, the NiNi crowdion must go in a NiCo dumbbell in Co plane that is 2.54 eV

Table 6
Activation barriers of SIA diffusion by translation-rotation mechanism in NiCu alloy depending on dumbbell composition and plane belonging. Barriers connecting in an unstable state are not indicated. Symmetrically-possible transition that do not exist due to instability of the initial or/and the final state, or because of the need for a non-available antisite in one of states are indicated as n/e. All values are in eV.

To\From		Ni plane			Cu plane		
		NiNi	NiCu	CuCu	NiNi	NiCu	CuCu
Ni plane	NiNi	n/e	n/e	n/e	0.04	0.16	n/e
	NiCu	n/e	n/e	n/e	n/e	0.03	0.08
	CuCu	n/e	n/e	n/e	n/e	n/e	n/e
Cu plane	NiNi	0.21	n/e	n/e	n/e	n/e	n/e
	NiCu	0.03	0.11	n/e	n/e	n/e	n/e
	CuCu	n/e	0.05	n/e	n/e	n/e	0.05

Table 7
Activation barriers of SIA diffusion by translation-rotation mechanism in NiCo alloy depending on dumbbell composition and plane belonging. Barriers connecting in an unstable state are not indicated. Symmetrically-possible transition that do not exist due to instability of the initial or/and the final state, or because of the need for a non-available antisite in one of states are indicated as n/e. All values are in eV.

To\From		Ni plane			Co plane		
		NiNi	NiCo	CoCo	NiNi	NiCo	CoCo
Ni plane	NiNi	n/e	n/e	n/e	0.43	2.41	n/e
	NiCo	n/e	n/e	n/e	n/e	0.15	0.12
	CoCo	n/e	n/e	n/e	n/e	n/e	n/e
Co plane	NiNi	0.11	n/e	n/e	n/e	n/e	n/e
	NiCo	0.19	0.20	n/e	n/e	0.13	0.14
	CoCo	n/e	0.79	n/e	n/e	0.39	n/e

Table 8
Effect of single defect kinetics on ordered nickel-based alloys at 300 K.

Single defect type/Disorder the alloy?	NiFe	NiCu	NiCo
Thermodynamically stable	Yes	No	No
Vacancy	No	Yes	Yes
Interstitial	No	Yes	No

above GS. At 300 K, once in meta1 state, the jump to meta2 is observed 14% of transitions (see Fig. 5). The other transitions, mostly connecting meta1 to meta1, involve the ⟨011⟩ diffusion of the NiNi dumbbell associated with a 2.53 Å displacement of the center of mass through crowdion motion in Ni layer; over the full simulation, we observe only two jumps connecting the meta2 state to the ground state. The lifetime of the $\langle 011 \rangle_{Ni}$-crowdion is equal to 2 picoseconds; due to high instability of the NiCo system, a many flickering states are observe.

Kinetically, therefore, CoCo and NiCo dumbbells transform into $\langle 001 \rangle_{Ni}$ NiNi dumbbells, generating Co antisites, that cost 1.21 eV, to reach the GS. From this point, diffusion is Ni dominated and restricted to the Ni plane, maintaining the $L1_0$ crystalline structure, irrespective of the initial interstitial. Due to symmetry of the system, a NiNi⟨001⟩ cannot translate-rotate to form the NiCo⟨100⟩, since this structure is unstable (Table 4). The GS can therefore only be reached in the presence of a Ni antisite in the Co layer. These barriers explain why, if disordering NiCo lowers its energy, as seen previously, this does not take place through interstitial diffusion on the 10^{-7} s timescale generated here at 300 K (Fig. 4(c) and (f)).

4. Discussion

Over the last few years, there have been significant efforts at characterizing the stability and evolution of metallic alloys [6,36,38]. In particular, the possibility of growing $L1_0$ NiFe, an alloy that presents promising magnetic properties, has caused many groups to address its stability and the role of self-defect in the order-disorder transition [5,7–9]. Running short high-temperature molecular dynamics simulations, above the order-transition temperature, for example, Chakraborty et al. identify a few barriers for vacancy for NiFe and show that disordering takes place at various rates in different alloys.

To fully understand the kinetic role of self-defects in the ordered phase, however, it is necessary to reconstruct in more details the energy lansdscape and follow the evolution of these defects on appropriate time scale, that can be well beyond the reach of molecular dynamics. Using the kinetic Activation-Relaxation Technique, we reconstructed the detailed energy landscape and kinetics of three fcc $L1_0$ alloys — NiFe, NiCo and NiCu — around single vacancies and self-interstitials (see Table 8, for a summary).

Starting with the $L1_0$ NiFe phase, which is stable below 600 K, we find that the monovacancy diffuses preferentially in the Fe planes, due to the slightly larger size of Fe atoms with respect to Ni. Since the Ni layer is under tension, the vacancy rapidly jumps into the Fe lattice, creating an antisite, that lowers the tension while also diminishing the compression in the Fe layer. Being confined, predominantly, in the Fe layer, vacancy diffusion does not affect the chemical arrangement of this structure, directly contributing to the observed stability of this crystal structure from DFT calculations [24] and experimental evidence [2,4].

For NiCo and NiCu alloys, for which the $L1_0$ phase is not observed experimentally, the chemical order is not conserved because of quasi-isotropic diffusion of vacancy. While NiCo disordering is dominated by energy relaxation, however, the evolution is NiCu is purely entropic.

Interstitial diffusion is also dramatically different in the three alloys and are coherent with the effects of vacancy diffusion. Contrary to vacancies, however, despite their similarities in terms of atomic size, interstitial migration pathways differ between alloys. Indeed, dumbbells in NiFe and NiCo alloys prefer to diffuse in Ni layers while the diffusion is quasi-isotropic in NiCu. This quasi-isotropy leads to a 3D diffusion of single defects in NiCu alloy, similar to what is observed in pure metals [10]. The $L1_0$ NiCu is therefore unstable under the diffusion of single vacancies and interstitials.

To a first approximation, vacancy and interstitial diffusion results can be explained by the size difference between the alloying elements [39]. Since Fe, Cu and Co are larger than Ni atoms, we could expect, if no other factor comes into play, the NiNi⟨001⟩ to present the highest stability as it makes us of the additional space along orientation. Fe being significantly larger than Ni, it is also natural to see, at low temperature, the vacancy move and diffuse predominantly in the Fe plane and dumbbells be confined to the Ni plane, making NiNi more stable than NiFe and FeFe dumbbells. Similarly, since size mismatch between Cu and Ni is only 2.5%, and both pure metals adopt the same fcc structure, we expect that both vacancy and and interstitial will move relatively isotropic fashion. The same logic should apply to NiCo alloys since size mismatch between Co and Ni is even smaller than between Cu and Ni. Electronic differences, here, as captured by the EAM potential, as supported by the agreement between our results and recent DFT calculation [34], seem to play a more important role, with the energetic largely favoring random configurations.

The complex self-interstitial diffusion mechanisms, observed in both in NiFe and NiCo, however, are multi-step processes that involve long-distance motion through metastable states that are not directly captured by a simple characterization of the energy barriers around GS configurations (Fig. 5). Self-interstitial diffusion is particularly intricate for NiCo, where diffusion from the first excited state, 0.30 eV above GS, is almost barrier-less. Moreover, we find that, for this system, the kinetics of SIAs plays against the thermodynamics: while solid solution NiCo is more energetically favorable than $L1_0$, the energy barriers considerably reduce the disordering through SIA motion.

We can compare this with the NiCu system, were diffusion is a single-step quasi-random process and takes place with translation-rotation mechanism. The quasi-random criteria is explained by the almost equal low diffusion barriers in different directions.

The atomic-thin network of tension and compressions zones created by size mismatch in the layer compounds is determinant the alloys' structural evolution: in NiFe, for example, defect motion is essential constrained to atomic plans while, for NiCo, for example, vacancy diffusion is mostly perpendicular to these planes, with macroscopic consequences. Indeed, this in-Fe-plane movement behavior, for example, implies that, in fcc $L1_0$ NiFe alloy, the dislocation glide a very low-probability process and the climb is a dominant one. However, because of higher probability of inter-plane plane diffusion in NiCo alloy, the climb encouraged against the glide.

In addition to the influence and effect of the presence of other defect type such as dislocation in pure [40] and composed metals [41], we show in our study that he symmetry and the order of the structure can play a major role in the movement dimensionality of point defects: For NiFe at room temperature, the alternated monolayer structure forces point defects to diffuse uniquely in one layer and thus the order is not affected by vacancy and interstitial diffusion, in agreement with experiment [14]; as expected, of course, raising the temperature eventually leads to an order-disorder transition. Self-defect diffusion, on the other hand, leads to the destabilisation, albeit through difference mechanisms, of the layer compound for both NiCu and NiCo, even at room temperature.

This study for the diffusion of single point defects allows us to understand some physical aspects not reported before, not only in $L1_0$, in other ordered structures such $L1_1$ and $L1_2$. This selective vacancy diffusion in NiFe, for example, play a role in the observed stabilization by Ni of the austenite phase. [42]

5. Conclusion

We have shown from longtime scale simulations using k-ART method that diffusion of point defects in apparently very similar nickel-based binary alloys — NiFe, NiCo and NiCu — shows different behavior that generate a diverse set of structural evolution pathways for the three systems. Focusing on $L1_0$ alloys, a highly ordered layered structure, allows us to fully characterize the energy landscapes of each system and assess the stability under self-defect diffusion. Through unbiased kinetic simulations performed on experimentally-relevant timescales, we have demonstrated that the movement of single vacancies does not affect the stability of ordered NiFe alloy due to in-Ni layer diffusion behavior. On the contrary, with different but quasi-isotropic movement, monovacancies rapidly destabilize NiCo and NiCu.

Interstitial diffusion is even richer: our results indicate a dominant bidimensional diffusion in NiFe alloy just was with the vacancy, and an isotropic tridimensional movement by translation-rotation mechanisms in NiCu and NiCo. However, while self-interstitial diffusion follows a straightforward mechanism, this is not the case for NiCo, which involves multiple intermediate steps.

We have shown here the richness associated the diffusion of point defects in newly relevant symmetric materials [2,4] with the help of methods that lift timescale limitations of standard methods and allow for extensive mapping of the system's energy landscape. This approach can also be used to treat the chemical arrangement dependency in disordered structures of these alloys which can allows us to understand in details clustering defects impact, radiation damage and corrosion problems at experimental timescales. Overall, these longtime scale simulations complementary provide informations not accessible by experiment and help us understand what is provide by methods such as y high-resolution transmission electron microscopy (HRTEM) [40,41,43], that are limited to 2D materials. Our results show a very rich and unexpected structural evolution led by size-mismatch as well as electronic constraints that cannot be obtained through a simple characterization of defect ground or even local energy barriers. These effects are profound and need to be further evaluated in the case of disordered structures as well as more complex alloys as we try to understand the physical original or clustering defects impact, radiation damage and corrosion problems in experimentally relevant conditions. They raise also the possibility to use this knowledge to design more stable or even self-annealing materials.

6. Code availability

Various ART nouveau implementations are available freely for download from http://www.normandmousseau.com. The k-ART and ART nouveau more recent codes are available from the authors upon request.

Acknowledgments

This work has been supported by the Canada Research Chairs program and by grants from the Natural Sciences and Engineering Research Council of Canada (NSERC) and the Fonds Québécois de la Recherche sur la Nature et les Technologies (FQRNT). We are grateful to Calcul Quebec for generous allocations of computer resources. SM is also thankful for financial support from the Tunisian government. We also thank M. M. Rahman and Roger Gaudreault for the important discussions that we did about this paper.

References

[1] S. Fukami, H. Sato, M. Yamanouchi, S. Ikeda, H. Ohno, Coni films with perpendicular magnetic anisotropy prepared by alternate monoatomic layer deposition, Appl. Phys. Express 6 (7) (2013) 073010 .
[2] K. Takanashi, M. Mizuguchi, T. Kojima, T. Tashiro, Fabrication and characterization of l10-ordered feni thin films, J. Phys. D Appl. Phys. 50 (48) (2017) 483002.
[3] C. Palmstrøm, Epitaxial heusler alloys: New materials for semiconductor spintronics, MRS Bull. 28 (10) (2003) 725–728.
[4] S. Goto, H. Kura, E. Watanabe, Y. Hayashi, H. Yanagihara, Y. Shimada, M. Mizuguchi, K. Takanashi, E. Kita, Synthesis of single-phase l10-feni magnet powder by nitrogen insertion and topotactic extraction, Sci. Rep. 7 (1) (2017) 13216.
[5] N. Bordeaux, A.M. Montes-Arango, J. Liu, K. Barmak, L.H. Lewis, Thermodynamic and kinetic parameters of the chemical order-disorder transformation in l10 feni (tetrataenite), Acta Mater. 103 (2016) 608–615.
[6] C. Lu, K. Jin, L.K. Béland, F. Zhang, T. Yang, L. Qiao, Y. Zhang, H. Bei, H.M. Christen, R.E. Stoller, et al., Direct observation of defect range and evolution in ion-irradiated single crystalline ni and ni binary alloys, Sci. Rep. 6 (2016) 19994.
[7] Y. Geng, T. Ablekim, M.A. Koten, M. Weber, K. Lynn, J.E. Shield, Defect generation and analysis in mechanically alloyed stoichiometric feni alloys, J. Alloys Compd. 633 (2015) 250–255, doi:10.1016/j.jallcom.2015.02.038.
[8] S. Zhao, G.M. Stocks, Y. Zhang, Defect energetics of concentrated solid-solution alloys from ab initio calculations: Ni 0.5 co 0.5, ni 0.5 fe 0.5, ni 0.8 fe 0.2 and ni 0.8 cr 0.2, Phys. Chem. Chem. Phys. 18 (34) (2016) 24043–24056.
[9] D. Chakraborty, A. Harms, M.W. Ullah, W. Weber, D. Aidhy, Effect of atomic order/disorder on vacancy clustering in concentrated nife alloys, Comput. Mater. Sci. 147 (2018) 194–203, doi:10.1016/j.commatsci.2018.02.011.
[10] S. Mahmoud, M. Trochet, O.A. Restrepo, N. Mousseau, Study of point defects diffusion in nickel using kinetic activation-relaxation technique, Acta Mater. 144 (2018) 679–690.
[11] F. El-Mellouhi, N. Mousseau, L.J. Lewis, Kinetic activation-relaxation technique: An off-lattice self-learning kinetic Monte Carlo algorithm, Phys. Rev. B 78 (15) (2008) 153202, doi:10.1103/PhysRevB.78.153202.
[12] N. Mousseau, L.K. Béland, P. Brommer, F. El-Mellouhi, J.F. Joly, G.K. N'tsouaglo, O.A. Restrepo, M. Trochet, Following atomistic kinetics on experimental timescales with the kinetic Activation Relaxation Technique, Comput. Mater. Sci. 100 (2015) 111–123, doi:10.1016/j.commatsci.2014.11.047.
[13] P. Brommer, L.K. Beland, J.F. Joly, N. Mousseau, Understanding long-time vacancy aggregation in iron: A kinetic activation-relaxation technique study, Phys. Rev. B Condens. Matter Mater. Phys. 90 (13) (2014) 1–9.
[14] L. Né el, J. Paulevé, R. Pauthenet, J. Laugier, D. Dautreppe, Magnetic properties of an iron-nickel single crystal ordered by neutron bombardment, J. Appl. Phys. 35 (1964) 873–876.
[15] S.M. Foiles, M.I. Baskes, M.S. Daw, Embedded-atom-method functions for the fcc metals Cu, Ag, Au, Ni, Pd, Pt, and their alloys, Phys. Rev. B 33 (12) (1986) 7983–7991, doi:10.1103/PhysRevB.33.7983.
[16] G. Barkema, N. Mousseau, Event-based relaxation of continuous disordered systems, Phys. Rev. Lett. 77 (21) (1996) 4358.
[17] R. Malek, N. Mousseau, Dynamics of lennard-jones clusters: A characterization of the activation-relaxation technique, Phys. Rev. E 62 (6) (2000) 7723.
[18] B.D. McKay, Practical Graph Isomorphism Department of Computer Science, Vanderbilt University Tennessee, US (1981).
[19] L.K. Béland, P. Brommer, F. El-Mellouhi, J.-F. Joly, N. Mousseau, Kinetic activation-relaxation technique, Phys. Rev. E 84 (4) (2011) 046704.
[20] M. Trochet, N. Mousseau, Energy landscape and diffusion kinetics of lithiated silicon: A kinetic activation-relaxation technique study, Phys. Rev. B 96 (13) (2017) 134118.
[21] E. Bitzek, P. Koskinen, F. Gähler, M. Moseler, P. Gumbsch, Structural relaxation made simple, Phys. Rev. Lett. 97 (17) (2006) 170201.
[22] K.J. Laidler, M.C. King, Development of transition-state theory, J. Phys. Chem. 87 (15) (1983) 2657–2664.
[23] L.K. Béland, P. Brommer, F. El-Mellouhi, J.-F. Joly, N. Mousseau, Kinetic activation-relaxation technique, Phys. Rev. E 84 (4) (2011) 046704.
[24] Y. Mishin, M. Mehl, D. Papaconstantopoulos, Phase stability in the feni system: Investigation by first-principles calculations and atomistic simulations, Acta Mater. 53 (15) (2005) 4029–4041.
[25] B. Onat, S. Durukanoğlu, An optimized interatomic potential for cuni alloys with the embedded-atom method, J. Phys. Conden. Matter 26 (3) (2013) 035404.
[26] P. Pietrokowsky, Lattice parameter of alpha iron by divergent beam diffraction, J. Appl. Phys. 37 (12) (1966) 4560–4571.
[27] E. Drexler, N. Simon, R. Reed, Properties of copper and copper alloys at cryogenic temperatures, Technical Report, NIST, 1992.

[28] F. Vincent, M. Figlarz, Quelques precisions sur les parametres cristallins et lintensite des raies debye-scherrer du cobalt cubique et du cobalt hexagonal, C. R. Hebd. Seances Acad. Sci. 264C (1967) 1270.
[29] G. Bonny, R. Pasianot, L. Malerba, Fe–ni many-body potential for metallurgical applications, Model. Simul. Mater. Sci. Eng. 17 (2) (2009) 025010.
[30] G. Bonny, D. Terentyev, R. Pasianot, S. Poncé, A. Bakaev, Interatomic potential to study plasticity in stainless steels: the fenicr model alloy, Model. Simul. Mater. Sci. Eng. 19 (8) (2011) 085008.
[31] G. Bonny, N. Castin, D. Terentyev, Interatomic potential for studying ageing under irradiation in stainless steels: the fenicr model alloy, Model. Simul. Mater. Sci. Eng. 21 (8) (2013) 085004.
[32] G.P. Pun, V. Yamakov, Y. Mishin, Interatomic potential for the ternary ni–al–co system and application to atomistic modeling of the b2–l10 martensitic transformation, Model. Simul. Mater. Sci. Eng. 23 (6) (2015) 065006.
[33] G. Bonny, R.C. Pasianot, N. Castin, L. Malerba, Ternary fe–cu–ni many-body potential to model reactor pressure vessel steels: First validation by simulated thermal annealing, Philos. Mag. 89 (34–36) (2009) 3531–3546.
[34] B. Liu, F. Yuan, K. Jin, Y. Zhang, W.J. Weber, Ab initio molecular dynamics investigations of low-energy recoil events in ni and nico, J. Phys. Condens. Matter 27 (43) (2015) 435006.
[35] R. Bourassa, B. Lengeler, The formation and migration energies of vacancies in quenched copper, J. Phys. F Metal Phys. 6 (8) (1976) 1405.
[36] S. Zhao, Y. Osetsky, Y. Zhang, Preferential diffusion in concentrated solid solution alloys: Nife, nico and nicocr, Acta Mater. 128 (2017) 391–399.
[37] P. Zhao, Y. Shimomura, Molecular dynamics calculations of properties of the self-interstitials in copper and nickel, Comput. Mater. Sci. 14 (1–4) (1999) 84–90.
[38] M. Müller, K. Albe, Kinetic lattice monte-carlo simulations on the ordering kinetics of free and supported fept l10-nanoparticles, Beilstein J. Nanotechnol. 2 (2011) 40.
[39] E. Clementi, D. Raimondi, W.P. Reinhardt, Atomic screening constants from scf functions. ii. atoms with 37 to 86 electrons, J. Chem. Phys. 47 (4) (1967) 1300–1307.
[40] K. Arakawa, K. Ono, M. Isshiki, K. Mimura, M. Uchikoshi, H. Mori, Observation of the one-dimensional diffusion of nanometer-sized dislocation loops, Science 318 (5852) (2007) 956–959.
[41] C. Lu, L. Niu, N. Chen, K. Jin, T. Yang, P. Xiu, Y. Zhang, F. Gao, H. Bei, S. Shi, et al., Enhancing radiation tolerance by controlling defect mobility and migration pathways in multicomponent single-phase alloys, Nat. Commun. 7 (2016) 13564.
[42] R. Klueh, P. Maziasz, E. Lee, Manganese as an austenite stabilizer in fe cr mn c steels, Mater. Sci. Eng. A 102 (1) (1988) 115–124.
[43] Z. Wu, Z. Ni, Spectroscopic investigation of defects in two-dimensional materials, Nanophotonics 6 (6) (2017) 1219–1237.